Triple-peak feature of Cu 2p x-ray-photoemission spectrum in copper acetylacetonate

Kozo Okada*

Institute for Solid State Physics, The University of Tokyo, 7-22-1 Roppongi, Minato-ku, Tokyo 106, Japan

Jun Kawai†

The Institute of Physical and Chemical Research (RIKEN), 2-1 Hirosawa, Wako, Saitama 351-01, Japan

Akio Kotani

Institute for Solid State Physics, The University of Tokyo, 7-22-1 Roppongi, Minato-ku, Tokyo 106, Japan

The Cu $2p$ x-ray-photoemission spectrum (XPS) of copper (II) acetylacetonate $Cu(acac)_2$ is measured. Both the $2p_{3/2}$ and $2p_{1/2}$ XPS show triple-peak features, which resemble the Ni $2p$ XPS in $NiCl_2$. By means of a cluster model, however, it is shown that the origin of the triple-peak feature in $Cu(acac)_2$ is quite different from that in Ni dihalides. In $Cu(acac)_2$, the main peak originates from one well-screened final state $(2p^53d^{10}\underline{L})$, where $\underline{L}$ denotes a ligand hole, while the two satellite peaks comes from the bonding and antibonding states between the other well-screened state and a poorly screened state $(2p^53d^9)$. The energy splitting in the $2p^53d^{10}\underline{L}$ states originates from strong hybridization between O $2p$ and C $2p$ orbitals.

I. INTRODUCTION

It has recently been accepted that x-ray-photoemission spectra (XPS) from transition metal (M) $2p$ core levels provide us with information on the local electronic structures in M's and their compounds. In the case of M monoxides,[1-5] the $2p$ XPS consists of an intense main peak and a satellite. The origin of the double-peak feature is the charge-transfer (CT) effect: In the final state of the XPS, the ligand electrons can be transferred to M $3d$ states in order to screen the core-hole charge. The well-screened and poorly screened final states correspond to the main peak and the satellite, respectively. By means of the cluster models,[6-15] it has been shown that the former and the latter are the $2p^53d^{n+1}\underline{L}$ and $2p^53d^n$ final states, respectively, where $\underline{L}$ denotes a ligand hole and $n = 9, 8, 7 \dots$ for Cu, Ni, Co, ...

Among M compounds, $NiCl_2$ and $NiBr_2$ are extraordinary in the sense that the Ni $2p$ XPS show triple-peak features.[7] It has been shown that in these compounds, an "overscreened" state $(2p^53d^{10}\underline{L}^2)$ can also have an appreciable XPS intensity. This situation occurs mainly because of a fairly small CT energy (Δ) from the ligand states to the Ni $3d$.[7,11,12] On going from Ni to Mn systems, Δ gradually increases, giving smaller XPS intensities to overscreened final states $(2p^53d^{n+2}\underline{L}^2)$.[4,5,14,15] In the case of divalent Cu compounds such as CuO, $CuCl_2$, and La_2CuO_4, there is no state corresponding to the overscreened state since the $3d$ states are already filled in the well-screened state. Accordingly, the Cu $2p$ XPS in divalent Cu compounds usually show double-peak features.[1,6]

On the other hand, the situation can be different for molecular systems. About two decades ago, it was pointed out that the Cu $2p$ XPS in some divalent Cu systems, such as copper (II) acetylacetonate $[Cu(acac)_2]$ and

$CuSO_4$, also reveal triple-peak features.[16,17] Although the observation by Perera, Frost, and McDowell[17] was done for gas-phase $Cu(acac)_2$, Kawai and Maeda[18] have found a similar triple-peak feature for solid-state $Cu(acac)_2$, which resembles the Ni $2p$ XPS in $NiCl_2$ and $NiBr_2$ at first glance. If the spectrum of $Cu(acac)_2$ is interpreted in analogy to those of the Ni compounds showing triple peaks, one arrives at the conclusion that Cu should have a $3d^8$ configuration in this material. However, this is ruled out by the first-principles molecular-orbital calculation for $Cu(acac)_2$, giving an electron configuration similar to $3d$ occupancies of typical divalent Cu compounds. (The details of the molecular-orbital calculations are given in a later section.) Thus, the triple-peak feature of Cu $2p$ XPS can be a challenging problem to the CT mechanism for the satellite formation in the $2p$ XPS. One of the purposes in the present paper is to confirm the triple-peak feature of the Cu $2p$ XPS in $Cu(acac)_2$, and the other is to find the origin.

The rest of the present paper is organized as follows: In Sec. II, we describe the details of the experiment and show the observed Cu $2p$ XPS for $Cu(acac)_2$. In Sec. III, we show the results of the discrete variational (DV)-$X\alpha$ molecular-orbital calculation for $Cu(acac)_2$, and explain the characteristic feature of the ground state. In Sec. IV, we describe our simplified cluster model, by which we calculate the Cu $2p$ XPS. It is well known that, in general, the first-principles calculations do not describe the excited states of actual materials quantitatively. In this paper, therefore, we adopt the cluster-model calculation, by which we calculated the core-level spectra for late M compounds.[9-14] We fix the parameter values introduced in the cluster model so that the observed $2p$ XPS can be reproduced, also referring to the result of the first-principles molecular-orbital calculation. In Sec. V, we show some calculated spectra and elucidate the origin of

TABLE I. Peak intensities and peak separations of Cu $2p_{3/2}$ XPS of Cu(acac)$_2$.

	A (main peak)		B (satellite)		C (satellite)
Intensity	52±2%		27±1%		22±1%
Peak separation		5.0±0.1 eV		4.8±0.1 eV	

the triple-peak feature of Cu $2p$ XPS. The simplified cluster model enables us to understand the essential point very clearly.

II. EXPERIMENT

The reagent-grade Cu(acac)$_2$ was obtained from Kanto Chemical Co., Inc., Japan. It was in powder form. The powder x-ray diffraction of it was measured to check the crystal structure. Although the degree of preferred orientation of the Cu(acac)$_2$ powder was very high, the x-ray-diffraction pattern agreed with the reference data in the JCPDS database.

The spectrometer used was a VG ESCA LAB MK II x-ray-photoelectron spectrometer (three-channeltron-detector type). Only the center channeltron data were used for XPS measurement to avoid the spectral distortion due to the nonequivalent response of the three channeltrons. The vacuum was 2×10^{-9} Torr during x-ray irradiation, and the base pressure was better than 8×10^{-10} Torr. The specimen was set on the sample holder by 3M double-sided adhesive tape. A Mg anode tube was used, with an applied power of 15 kV and 34 mA. Dwell time for one channel was 100 ms, and one channel was 0.20 eV. The pass energy was 50 eV. One spectrum was a

FIG. 1. Experimental and theoretical Cu $2p$ XPS for Cu(acac)$_2$. The spectrum consists of a pair separated by the Cu $2p$ spin-orbit splitting, each of which consists of three peaks. According to the present analysis, the main peak (A) originates from one $2p^5 3d^{10}\underline{L}$ final state. The other $2p^5 3d^{10}\underline{L}$ and $2p^5 3d^9$ states contribute to the two satellites (B,C). The spectral width of peak C is somewhat larger than that of peak B, reflecting the $2p^5 3d^9$ multiplet effect, which indicates that the $2p^5 3d^9$ character is somewhat larger in C than in B.

sum of five scans. The scanning was from 980 to 920 eV in binding energy. The measurements were taken at least three times to check the reproducibility. XPS spectra of Al $K\alpha$ excitation were also measured to check the contamination of unknown Auger peaks in the scanned energy region. Auger peaks were not detected in the Cu $2p$ region when excited by a Mg anode tube. The electron spectra were measured from the normal and a glancing angle by rotating the sample holder, since the Cu(acac)$_2$ molecule was planar, some effect due to the preferred orientation on the sample holder was expected. However, any significant differences were not detected between the normal- and the glancing-angle measured spectra. Although the Cu(acac)$_2$ powder sample was quite stable and the signals due to the surface adsorbates were negligibly weak, it took quite short time (30 sec) to obtain one spectrum avoiding the sample decompositions. Therefore, the weak signal was compensated by numerical smoothing. The obtained spectrum represents the electronic structure of the bulk state of Cu(acac)$_2$ powder.

The spectrum of Cu(acac)$_2$ without any data processing is shown in Fig. 1. In Table I, we show the peak separations and intensities with the standard deviations, which were estimated by the following numerical processing to reduce the standard deviations. The measured spectra were numerically smoothed by the Savitzky-Golay method[19] with five points, ten iterations, and then the Shirley background[20] was subtracted in the $2p_{3/2}$ region. Note here that the $K\alpha_{3,4}$ satellites were not subtracted, because the intensity was negligible (10% of $K\alpha_{1,2}$ main line) and the subtraction would introduce uncertainty. The absolute binding energies of the peaks were not determined because of the charge-up shift of the spectra.

III. FIRST-PRINCIPLES MOLECULAR-ORBITAL CALCULATION

As schematically shown in Fig. 2, a Cu atom in Cu(acac)$_2$ is surrounded by four O atoms in planar coordination, and the CuO$_4$ cluster is surrounded by four C atoms. In order to check the hybridization effect of C on the CuO$_4$ cluster, we calculated the electronic structure of Cu(acac)$_2$ molecules by means of the DV Hartree-Fock-Slater ($X\alpha$) molecular-orbital (MO) method.[21,22] The bond lengths used in the calculations were r(Cu-O)=1.96 Å, r(O-C)=1.27 Å, r(C-CH$_3$)=1.55 Å, r(C-CH)=1.48 Å, and r(C-H)=1.11 Å.[23] The basis set used was Cu $1s2s2p3s3p3d4s$, O $1s2s2p$, C $1s2s2p$, and H $1s$. The sampling point for the DV-$X\alpha$ calculation was 9000. The calculational details are similar to those reported in Refs. 24 and 25. The bars in Fig. 3 represent the content of the O $2p$ component in each eigenstate, which is equivalent to the partial density of states. The continu-
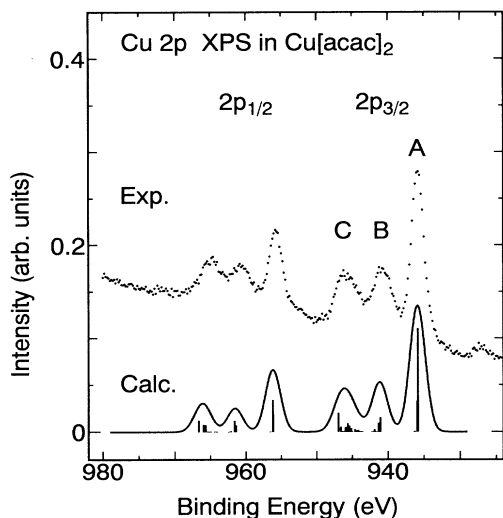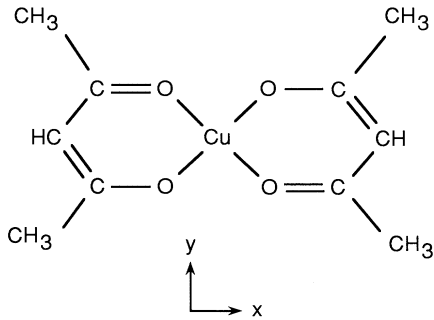
FIG. 2. The molecular structure of Cu(acac)$_2$ is schematically shown. A Cu atom is surrounded by four O atoms on the xy plane.

ous curves are convoluted from the bars with a Lorentzian function [full width at half maximum (FWHM) 1.0 eV].

In Fig. 3, we find that the centers of gravity for the O $2p_x$, $2p_y$, and $2p_z$ components differ considerably from each other. Of importance is the energy splitting of the $2p_x$ and $2p_y$ states, since they degenerate with each other in D_{4h} point symmetry. The energies of the O $2p_x$ states are greatly lowered because of the strong hybridization with the C $2p_x$ states, while the O $2p_y$ and $2p_z$ states are less affected by the C $2p$ states because of their π bonding. Incidentally, the antibonding state of O $2p_x$ and C $2p_x$ character is about 15 eV above the highest energy peak in Fig. 3. Consequently, the energy splitting of O $2p_x$ and $2p_y$ states is a characteristic feature of Cu(acac)$_2$, since this means that the Cu $3d(xy)$ orbital can hybridize with two molecular orbitals of significantly different energies. Actually, the Cu $3d(xy)$ content is appreciable for
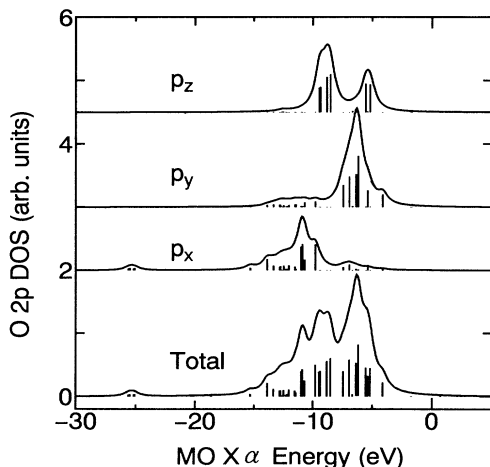

FIG. 3. The bar spectrum represents the O $2p$ content in each eigenstate which is obtained by the DV-$X\alpha$ molecular-orbital calculation (equal to the partial density of states). The abscissa is the MO $X\alpha$ energy. The continuous spectrum is convoluted from the bars with a Lorentzian function (FWHM 1.0 eV). Moreover, the O $2p$ components are decomposed into $2p_x$, $2p_y$, and $2p_z$ components.

the states with energy -4.0, -6.9, and -11.0 eV in Fig. 3. The first and second ones originate from the antibonding and bonding states of the Cu $3d(xy)$ and O $2p_y$ states. In the third one, on the other hand, the Cu $3d(xy)$ hybridizes with the bonding state between O $2p_x$ and C $2p_x$.

The characteristic feature of Cu(acac)$_2$ mentioned above should be compared with those of CuO and La$_2$CuO$_4$, where the hybridization of the $3d(xy)$ orbital to the O $2p$ bands in La$_2$CuO$_4$ (Ref. 26) and CuO (Ref. 27) is strongest at the top of the bands and its strength decreases rapidly with energy. [Note that the $3d(x^2-y^2)$ in Refs. 26 and 27 corresponds to the $3d(xy)$ in the present paper.] Therefore, we can safely approximate the valence bands in such solid systems as a single level, which is one reason why the square planar CuO$_4$ cluster model has so far been used successfully.[2,28] However, the situation is quite different for Cu(acac)$_2$. In the following, we show that the energy splitting of the O $2p_x$ and $2p_y$ states is essential in reproducing the triple-peak feature of the Cu 2p XPS.

IV. CLUSTER MODEL

We start with a square planar CuO$_4$ cluster model, by which two of the present authors (K.O. and A.K.) analyzed the Cu 2p XPS for CuO and La$_2$CuO$_4$.[9,10] The main part of the Hamiltonian is written as follows:

$$H = \sum_{\Gamma,\sigma} \varepsilon_d(\Gamma) d_{\Gamma\sigma}^{\dagger} d_{\Gamma\sigma} + \sum_{\nu} \varepsilon_p(\nu) c_{\nu}^{\dagger} c_{\nu}$$
$$+ \sum_{i,\Gamma,\sigma} \varepsilon_{vi}(\Gamma) v_{i\Gamma\sigma}^{\dagger} v_{i\Gamma\sigma}$$
$$+ \sum_{i,\Gamma,\sigma} V_i(\Gamma)(d_{\Gamma\sigma}^{\dagger} v_{i\Gamma\sigma} + v_{i\Gamma\sigma}^{\dagger} d_{\Gamma\sigma})$$
$$- U_{dc} \sum_{\Gamma,\sigma,\nu} c_{\nu} c_{\nu}^{\dagger} d_{\Gamma\sigma}^{\dagger} d_{\Gamma\sigma} , \qquad (1)$$

where, $d_{\Gamma\sigma}^{\dagger}$ and $c_{\nu}^{\dagger}$ create an electron on a Cu $3d$ state (with orbital symmetry Γ and spin σ) and on a Cu $2p$ state (with total angular momentum ν), respectively, and $v_{i\Gamma\sigma}^{\dagger}$ creates an electron on the ith O $2p$ molecular orbital. The first, second, and third terms in Eq. (1) represent the one-body energy parts for the Cu $3d$, Cu $2p$, and O $2p$ states, respectively. The fourth term describes the hybridization between the Cu $3d$ and O $2p$ states. The last term represents the Coulomb attraction between the core hole and the $3d$ electrons. The full Hamiltonian consists of Eq. (1), the multipole part of the Coulomb interaction, and the spin-orbit interaction.

We describe the ground state by a linear combination of $3d^9$ and $3d^{10}\underline{L}_i$ configurations, where $3d^9$ denotes the state where the Cu ion has a $3d^9$ electron configuration and the valence states are full. We define the CT energy from the ith valence state to the Cu $3d$ state as Δ_i. Accordingly, $E[3d^{10}\underline{L}_i] - E[3d^9] = \Delta_i$, with $E[3d^{10}\underline{L}_i]$ and $E[3d^9]$ being the configuration-average energies for $3d^{10}\underline{L}_i$ and $3d^9$, respectively. In the final state of XPS, the energy differences are changed by the core-hole potential as $E[2p^53d^{10}\underline{L}_i] - E[2p^53d^9] = \Delta_i - U_{dc}$.

Taking into account the hybridization effect of C $2p_x$

orbitals mentioned in Sec. III, we specify the Cu $3d$ states by the irreducible representations in D_{2h} symmetry. The $3d(xy)$ orbital is a b_{1g} irreducible representation in D_{2h}. Although the total number of the O $2p$ molecular orbitals is twelve, only two states of b_{1g} symmetry are important, which originate mainly from the O $2p_y$ and $2p_x$ states. Accordingly, we take $i = 1, 2$. Since the hybridization term in Eq. (1) conserves the orbital symmetry and the symmetry of the ground state is almost b_{1g}, the parameters that characterize the Cu $3d$ and O $2p$ states with symmetries other than b_{1g} hardly affect the calculated results shown below. For simplicity, we therefore disregard the i dependence of $\varepsilon_{vi}(\Gamma)$, and we use the relation

$$V_i(xy):V_i(3z^2 - r^2):V_i(x^2 - y^2):V_i(yz):V_i(zx)$$

$$= 1:1/\sqrt{3}:1/2:1/(2\sqrt{2}):1/(2\sqrt{2}) \ ,$$

which is an analog of the relation often used in the analysis of Cu $3d$ XPS (Refs. 2 and 28) and $2p$ XPS for CuO.[10]

The matrix elements for the multipole part of the Coulomb interaction and the spin-orbit interaction were numerically obtained by the Cowan[29] and Butler[30] computer programs, where the Slater integrals and the spin-orbit parameters were estimated by the Hartree-Fock (HF) calculation and the former were scaled down to 85% of their HF values. In terms of the Slater integrals, we can also describe the core-hole potential energy as $U_{dc} = F^0(2p, 3d) - (\frac{1}{15})G^1(2p, 3d) - (\frac{3}{70})G^3(2p, 3d)$, which is the average energy of the $2p$-$3d$ Coulomb interaction.[29] Since, however, it is well known that $F^0(2p, 3d)$ can be greatly reduced from the HF value due
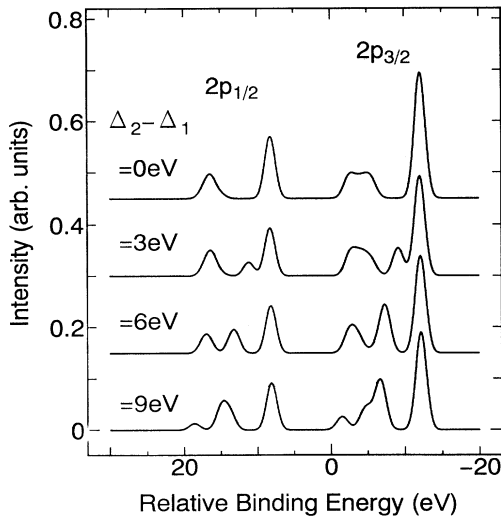

FIG. 4. Cu $2p$ XPS is shown as a function of $\Delta_2 - \Delta_1$, where the other parameters are fixed. (See text.) When $\Delta_2 - \Delta_1 = 0$ eV, the main peak and the satellite are due to the $2p^53d^{10}\underline{L}$ and $2p^53d^9$ final states, respectively, just as in CuO. With increasing $\Delta_2 - \Delta_1$, the $2p^63d^{10}\underline{L}$ final state splits. When $\Delta_2 - \Delta_1 = 6$ eV, the main peak is due to the $2p^53d^{10}\underline{L}_1$ final states, while the two satellites are due to the bonding and antibonding states of the $2p^53d^9$ and $2p^53d^{10}\underline{L}_2$ states.
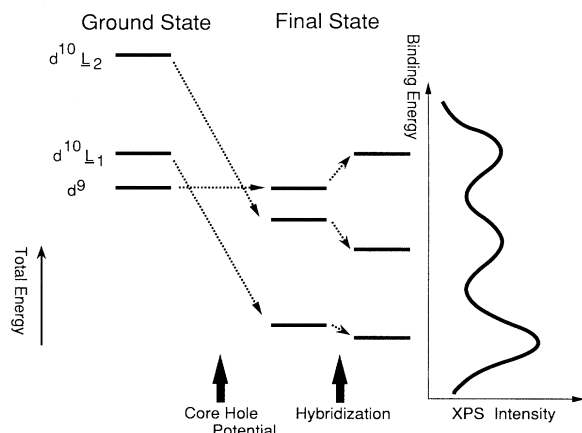
to various screening mechanisms, we treat U_{dc} as an adjustable parameter.

The photoemission intensity was calculated within the sudden approximation. The calculated spectra were broadened by convolution of a Gaussian function [of width 2.5 eV for Fig. 1 and 1.7 eV for Fig. 4 (FWHM)] to mimic the experimental spectra.

V. CALCULATED XPS SPECTRA

By the simplification mentioned above, the relevant parameters involved are Δ_1, Δ_2, $V_1(xy)$, $V_2(xy)$, and U_{dc}. $\Delta_2 - \Delta_1$ represents the energy splitting in the O $2p_x$ and $2p_y$ states. In the following calculations, we also took into account the crystal-field splitting of $3d$ levels ($10Dq = 0.5$ eV).

In Fig. 4, we show the $\Delta_2 - \Delta_1$ dependence of the Cu $2p$ XPS, where $V_1(xy) = V_2(xy) = 1.8$ eV, $\Delta_1 = 1.8$ eV, and $U_{dc} = 8$ eV are fixed. When $\Delta_2 - \Delta_1 = 0$ eV, the spectral shape of the Cu $2p$ XPS is almost the same as that in CuO.[10] Since $\Delta_2 = \Delta_1 < U_{dc}$, the $2p^53d^{10}\underline{L}_2$ and $2p^53d^{10}\underline{L}_1$ final states are degenerate in energy and are lower than the $2p^53d^9$ ones. Accordingly, the main peak corresponds mainly to the $2p^53d^{10}\underline{L}_2$ and $2p^53d^{10}\underline{L}_1$ final states. From the multiplet structure in the $2p_{3/2}$ XPS, we can also assign the satellite to the $2p^53d^9$ final states. In the case of $\Delta_2 - \Delta_1 = 3$ eV, there appears a small satellite in the higher-binding-energy side of the main peak, which is due mainly to the $2p^53d^{10}\underline{L}_2$ final state. With increasing $\Delta_2 - \Delta_1$, the satellite moves to higher binding energies and the $2p^53d^9$ multiplet structure is considerably distorted. In the case of $\Delta_2 - \Delta_1 = 9$ eV, it seems that the $2p^53d^{10}\underline{L}_2$ final state contributes mainly to the higher-energy satellite, since the lower-energy satellite in the $2p_{3/2}$ XPS shows a multiplet broadening.

Keeping in mind the parameter dependence of the Cu $2p$ XPS shown in Fig. 4, we readjusted the parameters to reproduce the observed spectrum as well as possible. The result obtained is shown in Fig. 1. The parameter values used for Fig. 1 were as follows: $V_1(xy) = V_2(xy) = 2$ eV, $\Delta_1 = 1.5$ eV, $\Delta_2 = 7.5$ eV, and $U_{dc} = 9$ eV. It seems that energy difference $\Delta_2 - \Delta_1 = 6$ eV is almost consistent with the result of the first-principles calculation, considering the hybridization effects. On the experimental spectrum, we can see that the width of the higher-energy satellite (peak C) in the $2p_{3/2}$ XPS is somewhat larger than that of the lower-energy one (peak B), which is consistent with our result. From Fig. 4, we can find that this is an effect of the $2p^53d^9$ multiplet structure and is evidence that Cu(acac)$_2$ is a "divalent" Cu system. Actually, the average $3d$ electron number in the ground state is 9.3 in our calculation, which is nearly the same as that obtained by the first-principles molecular-orbital calculation. To make the importance of the multiplet effects clear, we should compare Fig. 1 with the Ni $2p$ XPS in NiCl$_2$.[7] In NiCl$_2$, the higher-energy satellite splits due to the $2p^53d^8$ multiplet structure,[11,12] the line shape of which is considerably different from that of the Cu $2p$ XPS in Cu(acac)$_2$.

From Fig. 5, we can understand the origin of each

FIG. 5. Schematic total-energy diagram for Cu 2p XPS in Cu(acac)$_2$. The ground state is a heavy mixture of the $3d^9$ and $3d^{10}\underline{L}_1$ states, since their energy difference is fairly small. In the final state of XPS, the $3d^{10}\underline{L}_1$ and $3d^{10}\underline{L}_2$ states are lowered in energy because of the core-hole potential. As a result, the $3d^{10}\underline{L}_1$ state is much lower in energy than the $3d^9$, while the $3d^{10}\underline{L}_2$ is nearly degenerate with the $3d^9$, resulting in strong configuration mixing.

peak in Fig. 1: The ground-state wave function is a heavy mixture of the $3d^9$ and $3d^{10}\underline{L}_1$ states, while the weight of the $3d^{10}\underline{L}_2$ state is very small because of a large Δ_2. In the final state, the energies of the $2p^53d^{10}\underline{L}_2$ and $2p^53d^{10}\underline{L}_1$ states are lowered by U_{dc}. The $2p^53d^{10}\underline{L}_1$ state is much lower than the $2p^53d^9$ in energy, while the $2p^53d^{10}\underline{L}_2$ is very close to the $2p^53d^9$, since $\Delta_2 - U_{dc} = -1.5$ eV. Then the $2p^53d^{10}\underline{L}_2$ and $2p^53d^9$ states strongly hybridize with each other in the final state, and their bonding and antibonding states split by

about $2V_2(xy)$. As a result, the 2p XPS splits into three peaks, where the leading peak (A) originates mainly from the $2p^53d^{10}\underline{L}_1$ final state and the two satellites (B,C) are due primarily to the bonding and antibonding states of the $2p^53d^9$ and $2p^53d^{10}\underline{L}_2$ states. The $2p^53d^9$ character is somewhat stronger in C than in B, since $\Delta_2 - U_{dc} < 0$.

VI. CONCLUSION

We observed the Cu 2p XPS for Cu(acac)$_2$ and have clarified the origin of the triple-peak feature by means of a cluster model. With the CT mechanism, we can well reproduce the Cu 2p XPS in Cu(acac)$_2$. However, it is found that the origin of the triple-peak feature in Cu(acac)$_2$ is quite different from that in Ni compounds[7,11,12] and Ce compounds.[31,32] In the latter, the three peaks are due to poorly screened, well-screened, and overscreened final states. In Cu(acac)$_2$, on the other hand, the main peak is due to one well-screened final state ($2p^53d^{10}\underline{L}_1$), and the two satellites are due to the bonding and antibonding states of the other well-screened ($2p^53d^{10}\underline{L}_2$) and poorly screened states ($2p^53d^9$). The $2p^53d^9$ character is somewhat stronger in the higher-binding-energy satellite than in the lower-energy one. The energy splitting in the $2p^53d^{10}\underline{L}$ states originates from strong hybridization between the O $2p_x$ and C $2p_x$ states.

*Present address: Faculty of Education, Yamaguchi University, 1677-1, Yoshida, Yamaguchi 753, Japan.

†Present address: Department of Metallurgy, Kyoto University, Sakyo-ku, Kyoto 606, Japan.

[1]N. Nücker, J. Fink, B. Renker, D. Ewert, C. Politis, P. J. W. Weijs, and J. C. Fuggle, Z. Phys. B 67, 9 (1987).

[2]J. Ghijsen, L. H. Tjeng, H. Eskes, G. A. Sawatzky, and R. L. Johns, Phys. Rev. B 42, 2268 (1990).

[3]J. van Elp, R. H. Potze, H. Eskes, R. Berger, and G. A. Sawatzky, Phys. Rev. B 44, 1530 (1991).

[4]G. Lee and S.-J. Oh, Phys. Rev. B 43, 14 674 (1991).

[5]A. E. Bocquet, T. Mizokawa, T. Saitoh, H. Namatame, and A. Fujimori, Phys. Rev. B 46, 3771 (1992).

[6]G. van der Laan, C. Westra, C. Haas, and G. A. Sawatzky, Phys. Rev. 23, 4369 (1981).

[7]J. Zaanen, C. Westra, and G. A. Sawatzky, Phys. Rev. B 33, 8060 (1986).

[8]J. Park, S. Ryu, M. Han, and S.-J. Oh, Phys. Rev. B 37, 10 867 (1988).

[9]K. Okada and A. Kotani, J. Phys. Soc. Jpn. 58, 2578 (1989).

[10]K. Okada and A. Kotani, J. Electron Spectrosc. Relat.

Phenom. 53, 313 (1990).

[11]K. Okada and A. Kotani, J. Phys. Soc. Jpn. 60, 772 (1991).

[12]K. Okada, A. Kotani, and B. T. Thole, J. Electron Spectrosc. Relat. Phenom. 58, 325 (1992).

[13]K. Okada and A. Kotani, J. Phys. Soc. Jpn. 61, 445 (1992).

[14]K. Okada and A. Kotani, J. Phys. Soc. Jpn. 61, 4619 (1992).

[15]A. E. Bocquet, T. Saitoh, T. Mizokawa, and A. Fujimori, Solid State Commun. 83, 11 (1992).

[16]D. C. Frost, A. Ishitani, and C. A. McDowell, Mol. Phys. (GB) 24, 861 (1972).

[17]J. S. H. Q. Perera, D. C. Frost, and C. A. McDowell, J. Chem. Phys. 72, 5151 (1980).

[18]J. Kawai and K. Maeda, Physica C 185-189, 981 (1991).

[19]A. Savitzky and M. J. E. Golay, Anal. Chem. 36, 1627 (1964).

[20]D. A. Shirley, Phys. Rev. B 5, 4709 (1972).

[21]A. Rosén, D. E. Ellis, H. Adachi, and F. W. Averill, J. Chem. Phys. 65, 3629 (1976).

[22]C. Satoko, M. Tsukada, and H. Adachi, J. Phys. Soc. Jpn. 45, 1333 (1978).

[23]K. Ueno, Chelete Chemistry, An Introduction (Nankodo, Tokyo, 1988), pp. 92–97 (in Japanese).

[24]J. Kawai, Y. Nihei, M. Fujinami, Y. Higashi, S. Fukushima, and Y. Gohshi, Solid State Commun. **70**, 567 (1989).

[25]M. Sakai, S. Hayakawa, J. Kawai, and Y. Gohshi, Adv. X-Ray Anal. (to be published).

[26]A. K. McMahan, R. M. Martin, and S. Satpathy, Phys. Rev. B **38**, 6650 (1988).

[27]K. Karlsson, O. Gunnarsson, and O. Jepsen, J. Phys. Condens. Matter **4**, 2801 (1992).

[28]H. Eskes and G. A. Sawatzky, Phys. Rev. Lett. **61**, 1415 (1988).

[29]R. Cowan, *The Theory of Atomic Structure and Spectra* (University of California Press, Berkeley, 1981).

[30]P. H. Butler, *Point Group Symmetry Applications* (Plenum, New York, 1981).

[31]O. Gunnarsson and K. Schönhammer, Phys. Rev. B **28**, 4315 (1983).

[32]T. Jo and A. Kotani, J. Phys. Soc. Jpn. **55**, 2457 (1986).